# Wireless Sliding MPPT Control of Photovoltaic Systems in Distributed Generation Systems

**Aranzazu D. Martin \***[ID]**, Juan M. Cano, Reyes S. Herrera and Jesus R. Vazquez**

Departamento de Ingeniería Eléctrica y Térmica, de Diseño y Proyectos, University of Huelva,
21004 Huelva, Spain
**\*** Correspondence: aranzazu.delgado@die.uhu.es

**Abstract:** The aim of a photovoltaic (PV) system's control is the extraction of the maximum power even if the irradiance, the temperature, or the parameters vary. To do that, a maximum power point tracking (MPPT) algorithm is required. In this work, a sliding control is designed to regulate the PV modules' output voltage and make the panel work at the maximum power voltage. This control is selected to improve the robustness, the transient dynamic response, and the time response of the system under changeable environmental conditions, adjusting the duty cycle of the DC/DC converter. The DC/DC converter connected to the PV module output is a buck-boost converter. This configuration presents the advantage of providing voltages lower or higher than supplied by the photovoltaic modules to provide the required voltage to the load (including the voltages ceded by telecommunication loads, amongst others). In addition, a remote sliding control is developed to make the global supervision of the PV system in distributed generation grids. The designed algorithm is tested in an experimental platform, both locally and remotely connected to the base station, to prove the effectiveness of the sliding control. Thus, the communication effect in the control is also analyzed.

**Keywords:** photovoltaic system; maximum power point tracking (MPPT); sliding mode control; wireless communication

## 1. Introduction

The main objective of a photovoltaic (PV) system's control is power maximization. The voltage corresponding to the maximum power point (maximum power point voltage, MPPV) of each photovoltaic module (or set of modules) depends on the weather conditions. Thus, maximum power point tracking (MPPT) is needed. In plants located in places where there are fast changing environmental conditions, the tracking becomes critical [1], as well as in mobile plants, such as those associated to electrical vehicles, boats, or airplanes.

MPPT is an algorithm usually implemented in a power converter connected to the modules, which matches their optimal operating point with the load operation, [2–6]. It must be considered that load operation conditions can require lower or higher voltages than MPPV. In fact, telecommunications applications are quite suitable to be supplied by PV plants because telecom apparatus power consumption is approximately constant. Their nominal voltages work from 36 to 75 V, [7]. The majority of PV modules provide the output voltage within the range of 36 to 75 V. Thus, considering the available DC/DC converter topologies, [8], a buck-boost converter would be suitable as the adaptation device, [8]. In fact, this last configuration can supply voltages in the required range to the telecom equipment or even lower or higher voltages if it is necessary. The analysis and design of the buck-boost converters can be seen in [9,10].

Thus, the MPPT calculates the MPPV and the converter duty cycle (D) to make the modules work at the MPPV. Some algorithms in the technical literature achieves the objective with a control loop

as, for example, the perturb and observe (P&O) algorithm, the incremental conductance method, the ripple correlation control, or MPP trackers based on artificial neuronal networks, or fuzzy logic, [11–15]. These algorithms offer good performance. However, these solutions imply the use of linear controllers that decrease the bandwidth of the system and commits the global stability. The time response is also affected by that restriction when there are perturbations.

To overcome those problems, it must be considered that, actually, there are two control loops included in the MPPT. The first one calculates the MPPV from the weather conditions and the modules' characteristics. The second control loop calculates D to make the modules work at the MPPV. Additionally, the dynamic can be improved using specialized tracking algorithms to implement the second loop. These algorithms calculate the duty cycle of the DC/DC converter to make the modules voltage follow the MPPV previously calculated. Among these algorithms, the back-stepping, the sliding mode control (SMC), or others are considered, [16–19]. The use of one of these algorithms ensures an appropriate performance in the working range, operating in all the bandwidths of the system and guaranteeing global stability.

A comprehensive review and comparison of a variety of most-used MPPT methods is in [6,20,21], where the different control algorithms are classified regarding the complexity, true MPPT capability, number of sensors, and the variation of the parameters. The inherent nonlinearity of MPPT controllers makes it difficult to appreciate if the dynamic performance of each MPPT control algorithm is optimized or not. Indeed, the maximization of the convergence speed needs a commissioning phase to adjust the control method to the specific application in experimental implementations. Anyway, a fast convergence speed is always appreciable.

This paper focuses on the sliding mode control. This controller has been widely used for a variety of applications, such as robot manipulators, spacecrafts, underwater vehicles, electrical motors, etc., [22], and automotive applications such as anti-lock brake control, electronic throttle control, suspension control, and engine fault tolerant control, [23]. Besides, the use of the SMC in power systems is also extended, [24–29]. References [16,24,25] propose an adaption stage for a DC/DC converter regulated by a sliding mode control connected to an external MPPT algorithm, supplying the appropriate reference to the controller.

Reference [26] is focused on a new sliding mode control to enforce the adequate admittance to the PV array. This admittance is obtained tracking the reference given by an external admittance using a MPPT algorithm. In addition, the oscillations are mitigated in the DC-link and the use of voltage controllers is not required. In this case, a boost converter is used to raise the PV array voltage to the required value for the grid.

In the same line, [17] presents a fast and efficient MPPT algorithm for a PV system using back-stepping and sliding mode controllers. In addition, [27] presents a convergence study of a SMC of the MPPT using ripple correlation control. In both cases, the DC/DC converter considered is also a boost converter like in [28,29].

All those references only take into account the boost converter, keeping out important photovoltaic applications, such as those related to telecommunications, as explained above. To overcome this problem, in this paper the SMC is applied to a buck-boost converter integrated in a PV system supplying a resistive load. The SMC makes the modules track the MPPV calculated by an algorithm which previously obtains it. This algorithm applies a regression plane to obtain the reference voltage using a modified P&O, [30]. It avoids the local maximum points.

As an additional innovation, in this paper the control is implemented remotely and the communication effects are analyzed. In fact, a current tendency in the industry is the centralization of the control in remote control centers. The plants are monitored and the signals are sent to a server where the set points are calculated and returned to the plant. This tendency facilitates the maintenance revisions, among other advantages. In this sense, this paper makes a test of the proposed control implemented in a remote PC in communication with the local board connected to the converter in the outside platform.

Therefore, this paper is organized according to the next sections: In Section 2, the photovoltaic system used to test the algorithms is presented with the results of its simulation in Matlab/Simulink. In addition, the complete experimental system, locally or remotely connected, is presented. In Section 3, the proposed sliding control is described in a theoretical way. In Section 4, a use case is presented with the control implemented locally and in a remote way. Finally, in Section 5, some conclusions are drawn.

## 2. Photovoltaic System

The structure of the PV system is shown in Figure 1. It presents a PV system supplying a DC load through a DC/DC converter. The DC/DC converter is required to disengage the modules output voltage and the load input. Thus, a MPPT can be implemented as the DC/DC converter's control. In this way, the PV array is connected to the input of the DC/DC converter and the DC load is connected to the DC/DC converter's output. This configuration allows the converter voltage input to set at the required value to achieve the maximum power of the PV system. To do that, sensors are required to measure the voltages and currents at the DC/DC converter's input and output.
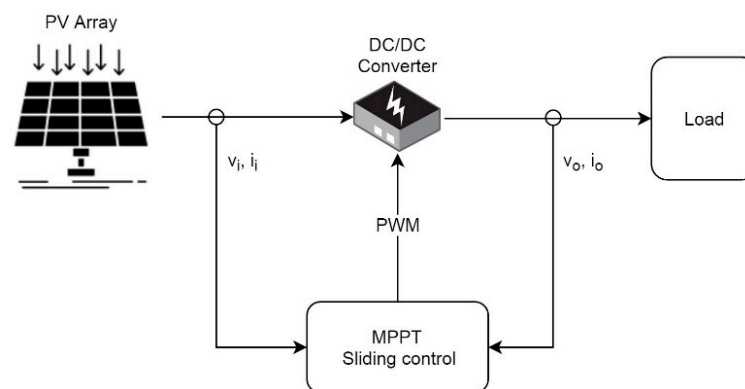
**Figure 1.** Structure of the photovoltaic (PV) system.

In this paper, a commercial PV module was chosen to be part of the experimental platform. Its features under standard conditions, 1000 W/m$^2$ and 25 °C, are detailed in Table 1. Amongst the others, the maximum power of this photovoltaic module is 20 W.

**Table 1.** Electrical parameters of the solar module.

| Parameter | Value |
|---|---|
| Maximum power ($P_{max}$), in Wp | 20 |
| Maximum power voltage ($V_{MPP}$), in V | 17.5 |
| Maximum power current ($I_{MPP}$), in A | 1.15 |
| Open-circuit voltage ($V_{OC}$), in V | 21.6 |
| Short-circuit current ($I_{SC}$), in A | 1.28 |

In addition, the module was previously simulated in Matlab-Simulink to obtain the characteristics curves, current–voltage (I–V) and power–voltage (P–V). Those curves are presented in Figure 2 with different irradiation conditions (simulation and experimental results). The model used in the simulation was presented by the authors in [31].
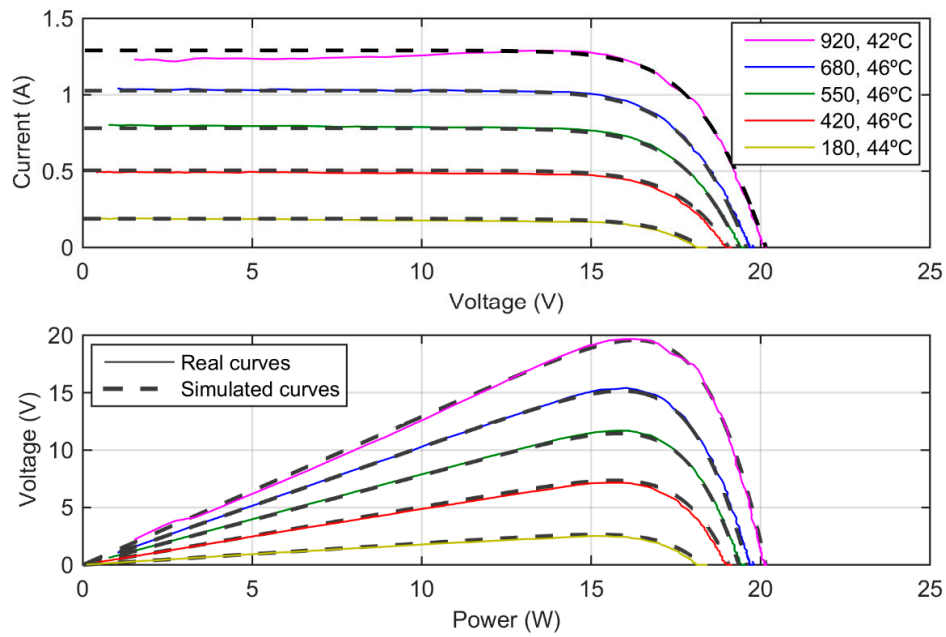
**Figure 2.** Current–voltage (I–V) and power–voltage (P–V) characteristic curves of a PV module.

With respect to the DC/DC converter, a buck-boost topology was designed to convert the voltage from one level to another lower or higher depending on the load requirements. Figure 3 represents the equivalent circuit of a buck-boost converter. As can be seen in the figure, the components of the buck-boost converter are two capacitors, an inductor, a transistor (in this case a MOSFET), *T1*, and a diode, *D2*. The use of the diode and the transistor implies the load works as a non-linear. In Figure 3, $v_{PV}$ is the PV output voltage or the buck-boost converter's input voltage in V, $i_{PV}$ is the PV modules' output current, $i_L$ is the inductor current, and $v_O$ is the DC/DC converter's output voltage, whereas $R$ is a resistor, $L$ an inductor, and *C1* and *C* are capacitors. They are constant parameters.
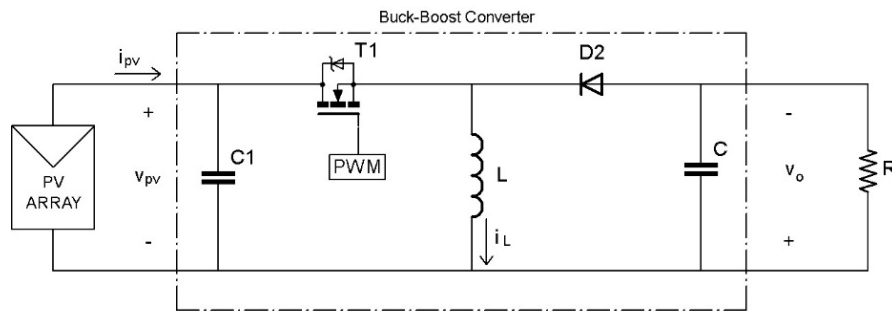


**Figure 3.** Buck-boost converter connected between the PV array and the load.

Regarding the control, the ON/OFF commutation of the switch allows the storage elements' charge and discharge energy to get the output voltage lower or higher than the input while it transfers the energy from the PV modules to the load. The converter duty cycle is $D = t_{ON}/t_C$, being $t_{ON}$ the time ON ($u = 1$) and $t_C$ the switching period within the range 0–1. The output:input ratio can be determined as follows in Equation (1).

$$\frac{v_O}{v_{PV}} = \frac{D}{1 - D}.\tag{1}$$

The state equations of the DC/DC open-loop buck-boost converter are presented in Equations (2)–(4).

$$\frac{dv_{PV}}{dt} = \frac{i_{PV}}{C_1} - \frac{i_L}{C_1}u. \qquad (2)$$

$$\frac{di_L}{dt} = -\frac{v_o}{L} + \frac{u}{L}(v_{PV} + v_o). \qquad (3)$$

$$\frac{dv_o}{dt} = \left(\frac{i_L}{C} - \frac{v_o}{RC}\right) - \frac{ui_L}{C}. \qquad (4)$$

The target of our control was to adjust the duty cycle to achieve the optimal voltage and to ensure the maximum energy extraction of the PV modules. A pulse width modulation (PWM) technique was used to control the transistor commutation. The output voltage presents the polarity opposite the input voltage. Figure 4 shows the voltages at the input and at the output of the buck-boost converter with different $D$ targets.
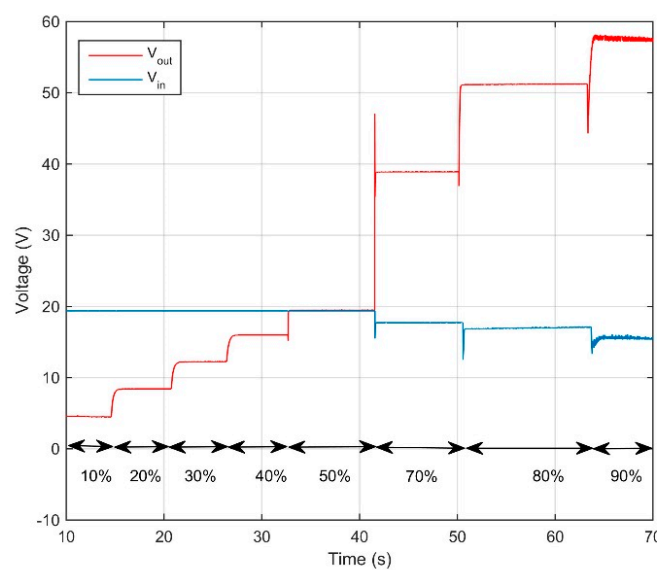


**Figure 4.** DC/DC converter's input and output voltages for some $D$ values.

The experimental platform contains three photovoltaic modules. The modules feed a built buck-boost converter (as the presented above) working with an input voltage of 10 V as minimum and 70 V as maximum. The maximum output voltage is 100 V. The maximum power that can be transferred is 70 W. The load is a 220 Ω resistor.

A personal computer (PC) is responsible for collecting the measurements and performing the control. LEM sensors are used to make the needed measurements. In this sense, the DC/DC converter includes three LA25NP current sensors to measure the input current, the output current, and the inductor current. Two LV25P voltage sensors measure the DC/DC converter's input and output voltage. A 12-bit digital analog converter, with a microcontroller 30F4011, manages all the sensors. The data obtained from the experiments is saved in the PC by means of a supervisory control and data acquisition (SCADA) system, which allows the figures to be presented using Matlab. The SCADA was designed in Visual Basic to visualize the data in real time and to implement the sliding controller remotely from a base station. The platform is depicted in Figure 5. Measurements are obtained through an EM203 serial-to-Ethernet module.

As a different possibility, a router with a wireless interconnection is included into the platform, to send the data via Wi-Fi. To do that, the base station running the application is required, with a Wi-Fi communication system using the user datagram protocol (UDP). Figure 6 presents the scheme of the interconnected system. The PC is connected to the router that allows the Wi-Fi communication and the

DC/DC converter is connected through the Ethernet interface RS232 to the router. The communication between DC/DC converter–PC are by Wi-Fi with a latency of 5 ms, Figure 7.
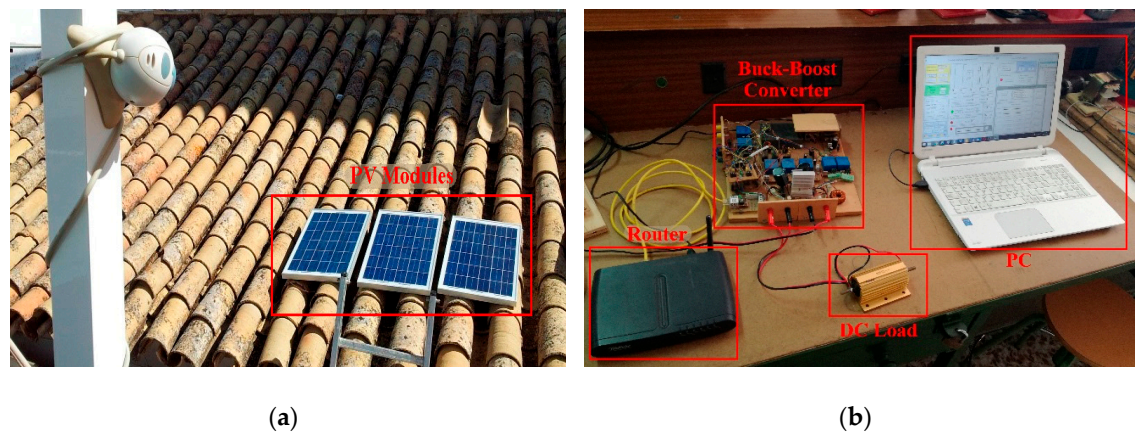


(**a**)                                          (**b**)

**Figure 5.** Experimental platform. (**a**) PV modules outside; (**b**) controller and base station.
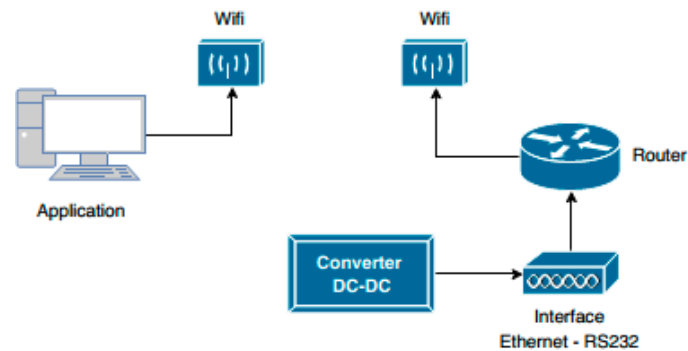


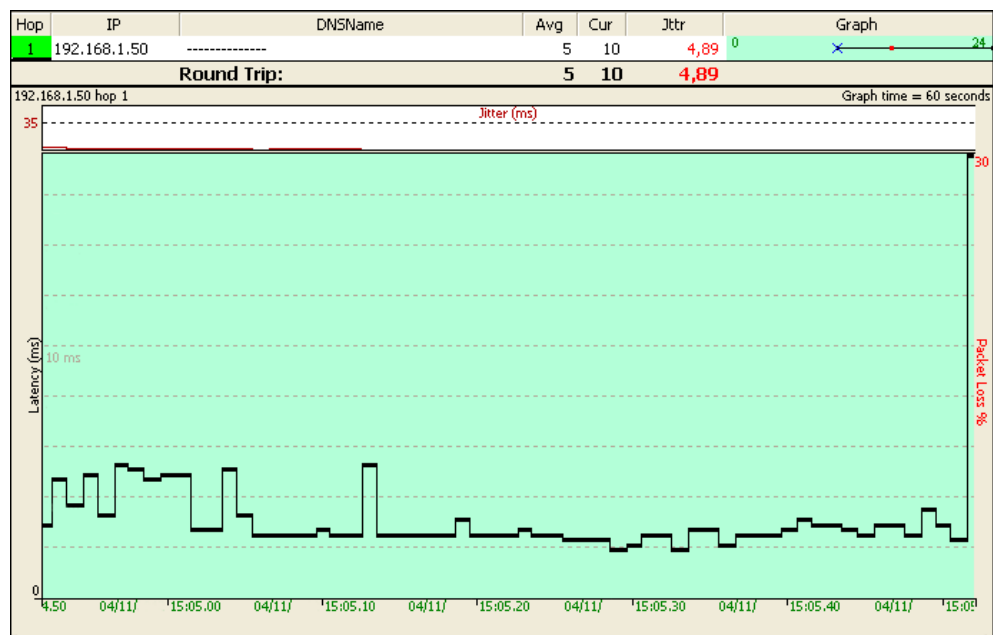**Figure 6.** Scheme of the interconnected system.



**Figure 7.** Round-trip latency in the wireless network.

Figure 7 shows the round-trip latency in the wireless network. The round-trip latency statistical value is 5 ms with a typical deviation of 1 ms.

## 3. Sliding Control

Several algorithms have been used up to now by the authors to control the DC/DC converter as a MPPT. The results of the back-stepping algorithm are presented in [29,30]. In both cases, results show that the controllers ensure maximum power transfer with changing irradiation conditions.

To improve the controller dynamic behavior, this work presents a non-linear sliding control method which is a variable structure controller. The sliding control will be applied to the buck-boost converter of a photovoltaic system because it is a variable structure system with a discontinuous control action, which modifies its structure to reach a set of switching surfaces. In addition, the buck-boost converter has a non-minimum phase structure. Then, the voltage must be controlled through the current.

The sliding control allows the buck-boost converter to work in a wide operating range obtaining a high dynamical performance. It uses a high speed switching law to make the system go to a predetermined sliding surface (or switching function). The switching law also makes the system remains in the surface. The dynamic behavior is given by the designed parameters and equations that define the switching surface. Thus, the sliding control is robust under disturbances and parameter variations.

To apply the sliding control, the buck-boost equations are defined using the state averaging method and the parameter $D$ when it works in continuous conduction mode (CCM).

$$\dot{x}_1 = \frac{i_{PV}}{C_1} - \frac{x_2}{C_1}D. \tag{5}$$

$$\dot{x}_2 = -\frac{x_3}{L} + \frac{(x_1 + x_3)}{L}D. \tag{6}$$

$$\dot{x}_3 = \frac{x_2}{C} - \frac{x_3}{RC} - \frac{x_2}{C}D. \tag{7}$$

$$\dot{x}_4 = x_4 \tag{8}$$

Then, the system equation is presented in (9).

$$\dot{x} = Ax + \delta + D(Bx + \gamma), \tag{9}$$

where $x = [x_1, x_2, x_3, x_4]^T$ with $x_1 = v_{PV}; x_2 = i_L; x_3 = v_o; x_4 = \int (v_{PV} - v_{PV}^r)dt$, $v_{PV}^r$ being the reference voltage to be reached.

These equations are rewritten in a matrix form as shown in Equation (10).

$$\dot{x} = Ax + \delta + D(Bx + \gamma). \tag{10}$$

The matrices are shown in Equations (11)–(14).

$$A = \begin{pmatrix} 0 & 0 & 0 & 0 \\ 0 & 0 & -\frac{1}{L} & 0 \\ 0 & \frac{1}{C} & -\frac{1}{RC} & 0 \\ 0 & 0 & 0 & 1 \end{pmatrix}. \tag{11}$$

$$\delta = \begin{pmatrix} \frac{i_{pv}}{C_1} \\ 0 \\ 0 \\ 0 \end{pmatrix}. \tag{12}$$

$$B = \begin{pmatrix} 0 & -\frac{1}{C_1} & 0 & 0 \\ \frac{1}{L} & 0 & \frac{1}{L} & 0 \\ 0 & -\frac{1}{C} & 0 & 0 \\ 0 & 0 & 0 & 0 \end{pmatrix}. \tag{13}$$

$$\gamma = \begin{pmatrix} 0 \\ 0 \\ 0 \\ 0 \end{pmatrix}. \tag{14}$$

A sliding surface with the dynamic suitable to this application is proposed in (15). Thus, the trajectories around the surface should converge to it and, then, the trajectories must stay on the sliding surface. In addition, the switching function ensures regulation of the buck-boost converter voltage.

$$S(x) = k_1(x_1 - v_{PV}{}^r) + x_2 + k_2 x_4, \tag{15}$$

where $k_1$ and $k_2$ are the sliding design parameters. The sliding surface exists if $S(x) = dS/dt = 0$.

Now, a control law to reach the sliding surface and stay thereafter must be found. It must also guarantee the existence of the sliding mode. The control input has two components called corrective control, $D_c$, and equivalent control, $D_{eq}$. Then, the control signal is presented in Equation (16).

$$D = D_c + D_{eq}. \tag{16}$$

The corrective control compensates the deviations from the sliding surface to reach the mentioned surface as shown in (17). It is a typical choice for this controller.

$$D_c = -k_c sgn(S), \tag{17}$$

where $k_c$ is chosen to be positive. The sign of the sliding surface is defined as shown in Equation (18).

$$sgn(S) = \begin{cases} +1, S(x) > 0 \\ -1, S(x) < 0 \end{cases}. \tag{18}$$

The equivalent control makes null the time derivative of the sliding surface to remain on the sliding surface. The equation that defines this control is presented in (19).

$$D_{eq} = -\left[\frac{\partial S}{\partial x}B(x)\right]^{-1}\left(\frac{\partial S}{\partial x}(Ax + \delta)\right). \tag{19}$$

Using Equations (9) and (15)–(17), the equivalent control can be expressed as shown in Equation (20).

$$D_{eq} = \frac{-k_1 L i_{PV} + C_1 x_3 - k_2 C_1 L x_4}{-k_1 L x_2 + C_1(x_1 + x_3)}. \tag{20}$$

It must fulfill Equations (21)–(23).

$$\frac{\partial S}{\partial x}Bx = -\frac{k_1 x_2}{C_1} + \frac{x_1 + x_3}{L} \neq 0. \tag{21}$$

$$-\left(\frac{\partial S}{\partial x}Bx\right)^{-1} = \frac{-C_1 L}{-k_1 L x_2 + C_1(x_1 + x_3)}. \tag{22}$$

$$\frac{\partial S}{\partial x}(Ax + \delta) = (k_1, 1, 0, k_2)\begin{pmatrix} \frac{i_{PV}}{C_1} \\ -\frac{x_3}{L} \\ \frac{x_2}{C} - \frac{x_3}{RC} \\ x_4 \end{pmatrix} = \frac{Lk_1 i_{PV} - C_1 x_3 + C_1 L k_2 x_4}{C_1 L}. \tag{23}$$

The buck-boost converter is working in CCM. Thus, the inductor current is always positive, $x_2$. Nevertheless, the output voltage is always negative, $x_3$. It is guaranteed if $k_1$ and $k_2$ are positive.

$S = 0$ is globally asymptotically stable. Thus, using Equations (16), (17), and (19), the control law is achieved. Its expression is presented in Equation (24).

$$D = \frac{-k_1 L i_{PV} + C_1 x_3 - k_2 C_1 L x_4}{-k_1 L x_2 + C_1 (x_1 + x_3)} - k_c sgn(S). \tag{24}$$

Now, a Lyapunov function, (25), is used to make the sliding mode control force the system to go to the sliding surface and remain on it.

$$V = \frac{1}{2}S^2. \tag{25}$$

To guarantee the stability of the system, the control $D$ has to be selected to make the time derivative of the Lyapunov function negative. Thus, the switching function will be attractive. Thus, the time derivative of the Lyapunov function is presented in Equation (26).

$$\dot{V} = S\dot{S} < 0,$$
$$\dot{V} = S\left(\frac{\partial S}{\partial x}(Ax + \delta) + \frac{\partial S}{\partial x}B(x)D\right). \tag{26}$$

Now, the time derivative of the sliding surface must be calculated, using Equation (27).

$$\dot{S}(x) = k_1(\dot{x}_1 - \dot{v}^r_{PV}) + \dot{x}_2 + k_2\dot{x}_4. \tag{27}$$

The time derivative of the Lyapunov function yields Equation (28).

$$\dot{V}(x) = S\dot{S} = S\left[k_1(\dot{x}_1 - \dot{v}^r_{PV}) + \dot{x}_2 + k_2\dot{x}_4\right]. \tag{28}$$

The term between square brackets is worked out, obtaining the expression shown in (29).

$$-k_1\dot{v}^r_{PV} - \frac{(x_1 + x_3)C_1 - x_2 L k_1}{C_1 L}k_c\frac{|S|}{S}. \tag{29}$$

The first term is considered to be zero. Then the time derivative of the Lyapunov function is presented in Equation (30).

$$\dot{V} = S\left(-\frac{x_1 C_1 + x_3 C_1 - x_2 L k_1}{C_1 L}k_c\frac{|S|}{S}\right) <$$
$$< -\frac{x_1 C_1 + x_3 C_1 - x_2 L k_1}{C_1 L}k_c|S| < 0. \tag{30}$$

The last term is negative. Then:

$$(x_1 C_1 + x_3 C_1 - x_2 L k_1)k_c < 0. \tag{31}$$

$$k_1 < \frac{(x_1 + x_3)C_1}{-x_2 L}. \tag{32}$$

These two equations close the sliding control.

## 4. Practical Cases

Experimental tests were carried out to validate the previous theoretical analysis of the sliding controller under different conditions. The experimental results were obtained with different scopes, both working in the experimental platform described in Section 2. In the first test, the physical system was wire connected to the PC and the second test was carried out with Wi-Fi communications, using a synthetic local wireless network.

### 4.1. Experimental Results with the Controller Connected to the PC by a Wire

The sliding control developed in this paper was implemented in a dsPIC30F4011 low-cost microcontroller, being supervised via a local internet connection. The sliding control has to regulate the DC/DC converter's input voltage to reach the MPP through the MOSFET switching controlling the duty cycle. The PWM frequency is 20 kHz whereas the sampling time of the control is 5 ms.

Experiments under different conditions were conducted to verify the sliding control performance. In this sense, there are different step signals that represent changes in the incident irradiance over the PV modules. Step signals were used to test the control, although the real irradiation changes are smooth due to the progressive appearance of the clouds. Thus, we tested the control in even worse conditions to verify the robustness. The system was tested with different irradiances, 670 W/m$^2$ until 33 s, 490 W/m$^2$ until 68 s, and 690 W/m$^2$ until 95 s, to finish with an irradiance of 330 W/m$^2$.

Figure 8 depicts the voltage and current transient response when there are step irradiance changes. Figure 8a shows the reference voltage to be achieved by the control at the PV modules' output or DC/DC converter's input, even when there are changes in the irradiance. The buck-boost converter's measured input voltage is shown in the figure, reaching the reference voltage values in all the cases. The DC/DC converter's output voltage is also presented in this figure. As expected, the converter's input voltage changes with the irradiance; both increase and decrease together.
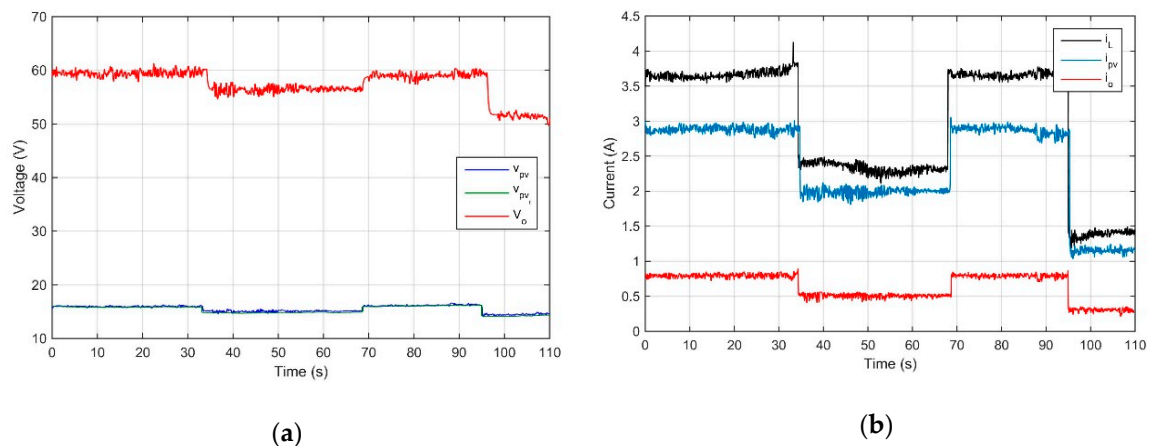


(**a**)  (**b**)

**Figure 8.** Transient response with variable irradiance with wire connection. (**a**) Converter's input and output voltage and reference voltage; (**b**) Inductor's current and converter's input and output currents.

The inductor's current and the converter's input and output currents are depicted in Figure 8b. These currents also change when the irradiance changes. As in the previous figure, the currents are higher when the irradiance achieves higher values and decrease when the irradiance is lower.

Figure 9 presents the output and input power of the DC/DC converter with the same changes in the irradiance as the voltages and current. This figure also defines the converter efficiency. The buck-boost converter efficiency ranges from 95% to 98.1% in this case. The voltages and the currents and; therefore, the power are robust, obtaining the expected values even when the irradiance changes suddenly, proving the robustness of the sliding control under external perturbation signals.
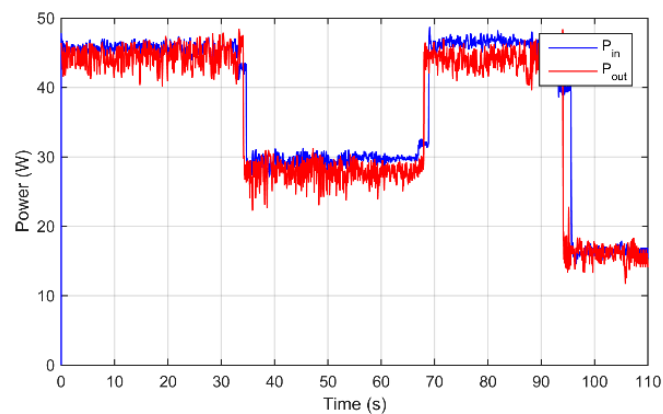
**Figure 9.** DC/DC converter's input and output power under variable irradiance with wire connection.

Results presented in Figures 8 and 9 are also shown in Table 2. In the simulation system, for the irradiance of 670 W/m$^2$, the maximum power is 45.1 W and the power obtained experimentally is 45 W; for 490 W/m$^2$, the maximum power is 30.1 W and the power obtained experimentally is 30.1 W; for 690 W/m$^2$, the maximum power is 46.3 W and the power obtained experimentally is 46.1 W; for 330 W/m$^2$, the values are 16.2 and 16.1 W, respectively. Thus, the MPPT efficiency ranges from 99.5% to 100%.

**Table 2.** Voltage and power values obtained at the converter's input and output under different irradiances with wire connection, time (s), G (W/m$^2$), $v_{PVr}$ is the reference voltage (V), $v_{PV}$ is the measured voltage at the DC/DC converter input (V), $v_o$ is the DC/DC converter output voltage (V), $P_{ref}$ is the reference power (W), $P_{in}$ is the DC/DC converter input power (W) and $P_{out}$ is the DC/DC converter output power (W).

| Time | G | $v_{PVr}$ | $v_{PV}$ | $v_o$ | $P_{ref}$ | $P_{in}$ | $P_{out}$ |
|---|---|---|---|---|---|---|---|
| [0, 33) | 670 | 15.8 | 15.8 | 59.5 | 45.1 | 45 | 42.9 |
| [33, 68) | 490 | 14.8 | 14.9 | 56.5 | 30.1 | 30.1 | 28.6 |
| [68, 95) | 690 | 15.9 | 15.9 | 58.8 | 46.3 | 46.1 | 43.9 |
| [95, 110] | 330 | 14.1 | 14.2 | 51.3 | 16.2 | 16.1 | 15.8 |

Figure 10 presents the control signal obtained using the sliding method. This figure shows the commuted control actions or the discontinuous actions needed to make the system remain in the sliding surface. It shows that the control signal changes its value when there is a change in the irradiance. It also presents the effect of the control non-linearities (the control is discontinuous).
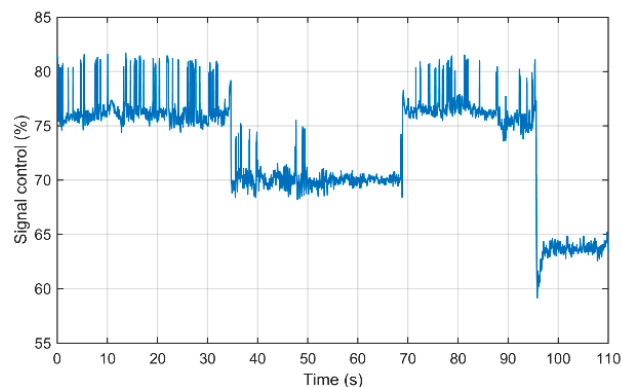


**Figure 10.** Control signal evolution with variable irradiance.

### 4.2. Experimental Results with the Controller Connected to the PC by Wireless Communication

To do this new test, the experimental platform used was the same as before. The only difference is that, now, the control is applied in a 2 GHz·PC with 4 GB·RAM. It is connected to the dsPIC via communication (IEEE802.11) through the UDP protocol at a nominal rate of 5 ms. This communication protocol is used because it is faster at sending data packets. The SCADA was also designed to implement the sliding controller remotely from the base station. The application receives the packet with the sensors' data from the dsPIC and the controller uses those data to calculate the control signal, which is packaged and sent to the microcontroller to update the PWM that controls the buck-boost converter.

In these new conditions of wireless connection, the sliding control robustness is tested again, using the same set of experiments as in the previous case, with the same sudden changes in the irradiance. The irradiance is 200 W/m$^2$ until 1 s, 360 W/m$^2$ until 9 s, 470 W/m$^2$ until 18 s, 760 W/m$^2$ until 24 s, 480 W/m$^2$ until 33 s, 780 W/m$^2$ until 36 s, 480 W/m$^2$ until 42 s, and 780 W/m$^2$ again until 45 s.

Figure 11 presents, as in the previous case, the transient response of the voltages, currents, and powers under sudden changes in the irradiance. Figure 11a presents the reference voltage that has to be reached, the DC/DC converter's input voltage that follows the reference voltage, and the buck-boost converter's output voltage. Figure 11b depicts the inductor's current and the DC/DC converter's input and output currents.
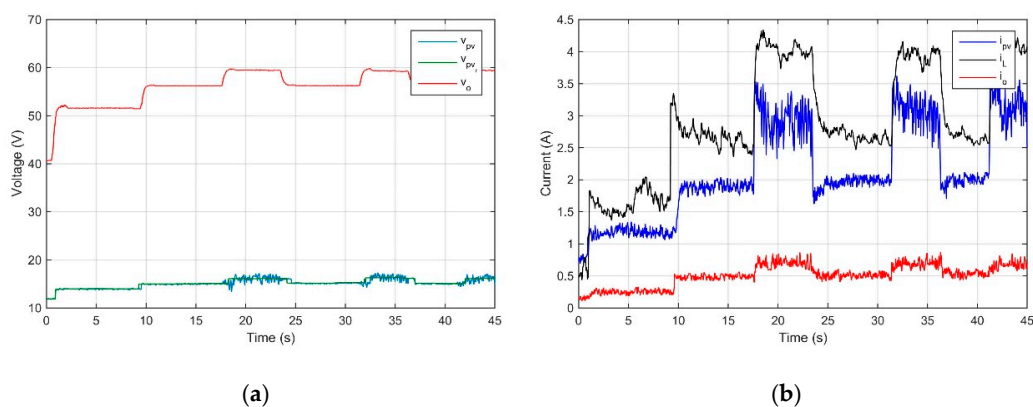


(**a**)                                                                                         (**b**)

**Figure 11.** Transient response with variable irradiance with wireless connection. (**a**) Converter's input and output voltage and reference voltage; (**b**) Inductor's current and converter input and output currents.

Then, Figure 12 shows the power at the input and output buck-boost converter, defining the converter efficiency. In this case, the efficiency of the DC/DC converter ranges from 93.2% to 94%. As in the previous case, the voltage, current, and power values increase when the irradiance increase, whereas the values decreases when the irradiance goes down. Table 3 summarizes those results.
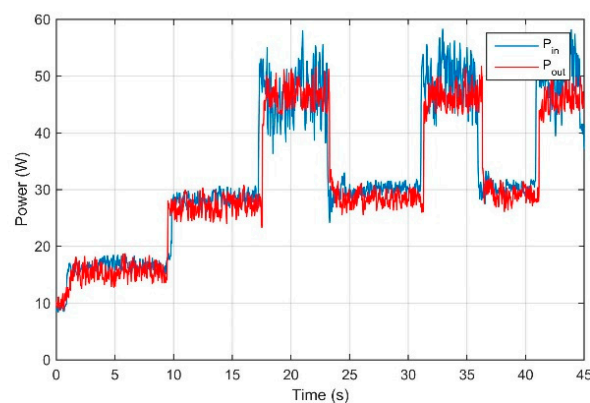


**Figure 12.** DC/DC converter's input and output power under variable irradiance with wireless connection.

**Table 3.** Voltage and power values obtained at the converter's input and output under different irradiances, time (s), G (W/m$^2$), and V (V) with Wi-Fi.

| Time | G | $v_{PVr}$ | $v_{PV}$ | $v_o$ | $P_{ref}$ | $P_{in}$ | $P_{out}$ |
|---|---|---|---|---|---|---|---|
| [0, 1) | 200 | 11.90 | 11.90 | 40.7 | 9.8 | 9.7 | 9.1 |
| [1, 9) | 360 | 14.02 | 14.02 | 51.6 | 17 | 16.9 | 15.9 |
| [9, 18) | 470 | 15.01 | 15.01 | 56.1 | 29.2 | 28.9 | 27.1 |
| [18, 24) | 760 | 16.1 | 16.1 | 59.4 | 48 | 47.9 | 44.8 |
| [24, 33) | 480 | 15.1 | 15.1 | 56.2 | 29.8 | 29.6 | 27.6 |
| [33, 36) | 780 | 16.2 | 16.2 | 59.2 | 49 | 48.8 | 45.7 |
| [36, 42) | 480 | 15.1 | 15.1 | 56.2 | 29.8 | 29.7 | 27.7 |
| [42, 45] | 780 | 16.2 | 16.2 | 59.2 | 49 | 48.9 | 45.9 |

As expected, the wireless communication makes the signals in Figure 12 have more noise than that obtained in the previous case (Figure 9) due to the wireless communication effect. Indeed, this type of communication implies a variable delay in the signal processing and data transmission. The data are packaged with the sensors information to be sent from the DC/DC converter to the base station, and the packaged data with the control signal information are sent from the base station to the buck-boost converter. However, in spite of the higher delay, the control remains stable and the variables converge to the set points. Thus, the sliding control robustness is verified.

The delay in the data processing and the data transmission packets with the packaged data from the microcontroller to the base station, and vice versa, are depicted in Figure 13. These measurements were taken when the experiment was conducted. The values were obtained independently from the PC and from the dsPIC, showing a mean value of time of 5.4 ms.
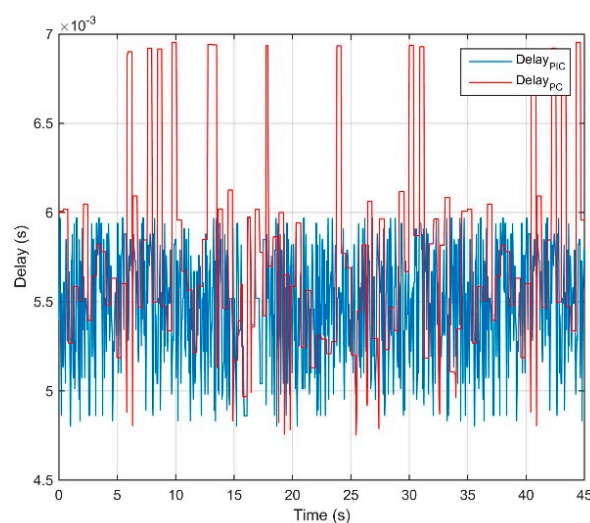


**Figure 13.** Delay of the variables time response and number of lost packages.

Figure 14 presents the control signal. As in Figures 11 and 12, it is shown that the control changes when the irradiance changes as well, in order to make the system remain in the sliding surface. It also depicts the effect of the discontinuous control non-linearities, but in this case with more noise.
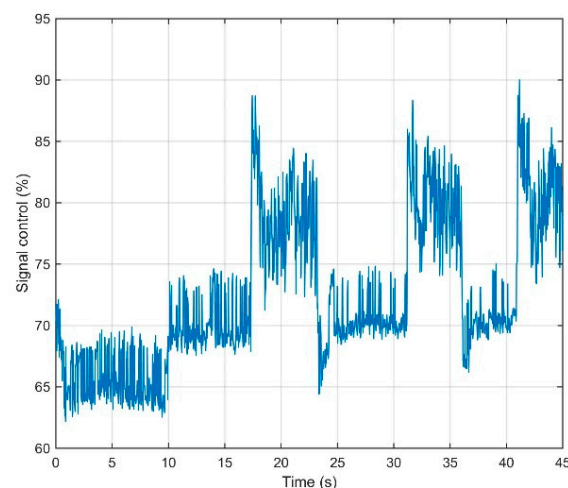
**Figure 14.** Control signal evolution with a variable irradiance through wireless communication.

In all the figures presented in this subsection, in the wireless network case, the signals present more oscillations and the efficiency of the DC/DC converter is lower (from 98.1% to 94% as maximum efficiency) than that corresponding to the previous case with wire connection. In fact, control algorithms present a delay due to the time necessary to process the signals and make the suitable operations. The delay grows in wireless connection because of the time necessary to transmit the data. The delay is also affected by the distance between the buck-boost converter and the base station and by the interferences created by other systems that use the same frequency. As the delay increased, the system efficiency decreased. Moreover, the variability of the transmission time provokes a higher noise in all the electrical signals in the case of wireless connection. Even so, the controller reaches the desired values and; therefore, it can be used in centralized systems.

## 5. Conclusions

In this paper, the sliding mode control was applied to make a set of photovoltaic modules track the maximum power point voltage. The use of this control improved the dynamics of the system and its response to perturbations in the load or in the irradiance. The control algorithm was implemented in a buck-boost converter, which is able to supply a voltage lower and higher than the input voltage, as required by telecommunications applications, amongst others. To achieve it, a boost converter is not suitable. In addition, the algorithm was experimentally tested in a platform with the controller remotely connected to the photovoltaic systems and the effect of the distance was evaluated. The system proved to be efficient with both wire and wireless communication, and in both cases the dynamic performance was improved. The communications effect provides a higher level of noise although the dynamics remain good. In addition, the buck-boost converter's efficiency decreases from 98.1% to 94% in the case of remote control, but the control remains stable and the voltage reference is reached with an efficiency between 99% to 99.8%, proving the wireless control works in centralized photovoltaic plants and in distributed generation systems.

## References

1.  Çelik, Ö.; Teke, A. A Hybrid MPPT method for grid connected photovoltaic systems under rapidly changing atmospheric conditions. *Electr. Power Syst. Res.* **2017**, *152*, 194–210. [CrossRef]
2.  Femia, N.; Petrone, G.; Spagnuolo, G.; Vitelli, M. Optimization of perturb and observe maximum power point tracking method. *IEEE Trans. Power Electron.* **2005**, *20*, 963–973. [CrossRef]
3.  Sera, D.; Mathe, l.; Kerekes, T.; Spataru, S.V.; Teodorescu, R. On the Perturb-and-Observe and Incremental Conductance MPPT Methods for PV Systems. *IEEE J. Photovolt.* **2013**, *3*, 1070–1078. [CrossRef]
4.  Fernandes, D.; Almeida, R.; Guedes, T.; Filho, A.J.S.; Costa, F.F. State feedback control for DC-photovoltaic systems. *Electr. Power Syst. Res.* **2017**, *143*, 794–801. [CrossRef]
5.  Masoum, M.A.S.; Dehbonei, H.; Fuchs, E.F. Theoretical and experimental analyses of photovoltaic systems with voltage and current-based maximum power-point tracking. *IEEE Trans. Energy Convers.* **2002**, *17*, 514–522. [CrossRef]
6.  Islam, H.; Mekhilef, S.; Shah, N.B.M.; Soon, T.K.; Seyedmahmousian, M.; Horan, B.; Stojcevski, A. Performance Evaluation of Maximum Power Point Tracking Approaches and Photovoltaic Systems. *Energies* **2018**, *11*, 365. [CrossRef]
7.  Ren, X.; Tang, Z.; Ruan, X.; Wei, J.; Hua, G. Four Switch Buck-Boost Converter for Telecom DC-DC power supply applications. In Proceedings of the Twenty-Third Annual IEEE Applied Power Electronics Conference and Exposition, Austin, TX, USA, 24–28 February 2008; pp. 1527–1530.
8.  *Power Electronics Handbook*; Elsevier: Amsterdam, The Netherlands, 2018.
9.  Pradeep, A.; Yadav, K.; Thirumalia, S.; Haritha, G. Comparison of MPPT Algorithms for DC-DC Converters Based PV Systems. *Int. J. Adv. Res. Electr. Electron. Instrum. Eng.* **2012**, *1*, 18–23.
10. Babaei, E.; Mahmoodieh, M.E.S.; Mahery, H.M. Operational Modes and Output-Voltage-Ripple Analysis and Design Considerations of Buck-Boost DC-DC Converters. *IEEE Trans. Ind. Electron.* **2012**, *59*, 381–391. [CrossRef]
11. Tan, B.; Ke, X.; Tang, D.; Yin, S. Improved Perturb and Observation Method Based on Support Vector Regression. *Energies* **2019**, *12*, 1151. [CrossRef]
12. Tey, K.S.; Mekhilef, S. Modified incremental conductance MPPT algorithm to mitigate inaccurate responses under fast-changing solar irradiation level. *Sol. Energy* **2014**, *101*, 333–342. [CrossRef]
13. Esram, T.; Kimball, J.W.; Krein, P.T.; Chapman, P.L.; Midya, P. Dynamic maximum power point tracking of photovoltaic arrays using ripple correlation control. *IEEE Trans. Power Electron.* **2006**, *21*, 1282–1291. [CrossRef]
14. Elobaid, L.M.; Abdelsalam, A.K.; Zakzouk, E.E. Artificial neural network-based photovoltaic maximum power point tracking techniques: A survey. *IET Renew. Power Gener.* **2015**, *9*, 1043–1063. [CrossRef]
15. Guenounou, O.; Dahhou, B.; Chabour, F. Adaptive fuzzy controller based MPPT for photovoltaic systems. *Energy Convers. Manag.* **2014**, *78*, 843–850. [CrossRef]
16. Montoya, D.G.; Paja, C.A.R.; Giral, R. Maximum power point tracking based on the sliding mode control of the average PV admittance. In Proceedings of the 2014 IEEE Emerging Technology and Factory Automation (ETFA), Barcelona, Spain, 16–19 September 2014; pp. 1–5.
17. Dahech, K.; Allouche, M.; Damak, T.; Tadeo, F. Backstepping sliding mode control for maximum power point tracking of a photovoltaic system. *Electr. Power Syst. Res.* **2017**, *143*, 182–188. [CrossRef]
18. Vazquez, J.R.; Martin, A.D. Backstepping Control of a Buck-Boost Converter in an Experimental PV-System. *J. Power Electron.* **2015**, *15*, 1584–1592. [CrossRef]
19. Martin, A.D.; Cano, J.M.; Silva, J.F.A.; Vázquez, J.R. Backstepping Control of Smart Grid-Connected Distributed Photovoltaic Power Supplies for Telecom Equipment. *IEEE Trans. Energy Convers.* **2015**, *30*, 1496–1504. [CrossRef]
20. Salah, C.B.; Ouali, M. Comparison of fuzzy logic and neural network in maximum power point tracker for PV systems. *Electr. Power Syst. Res.* **2011**, *81*, 43–50. [CrossRef]
21. Ezinwannea, O.; Zhongwena, F.; Zhijunb, L. Energy Performance and Cost Comparison of MPPT Techniques for Photovoltaics and other Applications. In Proceedings of the 3rd International Conference on Energy and Environment Research (ICEER), Barcelona, Spain, 7–11 September 2016.
22. Wu, L.; Yang, R.; Sun, G.; Zhao, X.; Shi, P. New Developments in Sliding Mode Control and Its Applications. *Math. Probl. Eng.* **2015**. [CrossRef]

23. Fu, L.; Özgüner, Ü.; Haskara, I. Automotive Applications of Sliding Mode Control. *IFAC Proc. Vol.* **2011**, *44*, 1898–1903. [CrossRef]

24. Haroun, R.; Aroudi, A.E.; Cid-Pastor, A.; Garcia, G.; Olalla, C.; Martínez-Salamero, L. Impedance Matching in Photovoltaic Systems Using Cascaded Boost Converters and Sliding-Mode Control. *IEEE Trans. Power Electron.* **2015**, *30*, 3185–3199. [CrossRef]

25. Mamarelis, E.; Petrone, G.; Spagnuolo, G. A two-steps algorithm improving the P&O steady state MPPT efficiency. *Appl. Energy* **2014**, *113*, 414–421.

26. Montoya, D.G.; Paja, C.A.R.; Giral, R. Maximum power point tracking of photovoltaic systems based on the sliding mode control of the module admittance. *Electr. Power Syst. Res.* **2016**, *136*, 125–134. [CrossRef]

27. Costabeber, A.; Carraro, M.; Zigliotto, M. Convergence Analysis and Tuning of a Sliding-Mode Ripple-Correlation MPPT. *IEEE Trans. Energy Convers.* **2015**, *30*, 696–706. [CrossRef]

28. Valencia, P.A.O.; Ramos-Paja, C.A. Sliding-Mode Controller for Maximum Power Point Tracking in Grid-Connected Photovoltaic Systems. *Energies* **2015**, *8*, 12363–12387. [CrossRef]

29. Ramos-Paja, C.A.; Montoya, D.G.; Rodriguez, J.D.B. Sliding-Mode Control of Distributed Maximum Power Point Tracking Converters Featuring Overvoltage Protection. *Energies* **2018**, *11*, 2220. [CrossRef]

30. Martin, A.D.; Vazquez, J.R. Backstepping Controller Design to Track Maximum Power in Photovoltaic Systems. *Automatika* **2014**, *55*, 22–31. [CrossRef]

31. Martin, A.D.; Vazquez, J.R.; Cano, J.M. MPPT in PV Systems under Partial Shading Conditions using Artificial Vision. *Electr. Power Syst. Res.* **2018**, *162*, 89–98. [CrossRef]